THE ASTROPHYSICAL JOURNAL, 274:611–631, 1983 November 15

H II REGIONS AND STAR FORMATION IN M83 AND M33

K. S. RUMSTAY
Astronomy Department, The Ohio State University
AND
MICHELE KAUFMAN
Physics Department, The Ohio State University
Received 1982 December 20; accepted 1983 April 20

ABSTRACT

A catalog listing positions, fluxes, and isophotal diameters of 296 H II regions in M83 is compiled from the Hα observations of Talbot, Jensen, and Dufour. The luminosity function for H II regions in M83 does not look like a simple power law and, in this respect, does not resemble the luminosity functions published for M33 and NGC 628; however, the data for NGC 628 generally referred to larger, more luminous regions. In M83, giant H II regions (excitation parameter $U > 115$ pc cm^{-2}) differ from nongiant H II regions ($U < 115$ pc cm^{-2}) in both azimuthal and radial distribution in the plane of the galaxy. We find a similar phenomenon in M33 by using the lists of H II regions published by Boulesteix *et al.* and by Israel and van der Kruit. In both galaxies, (*i*) the two-armed spiral pattern shows up more clearly in the distribution of giant H II regions; (*ii*) the rms scale of the radial distribution of H II regions is larger for nongiant than for giant regions; and (*iii*) the *e*-folding length of the radial distribution predicted for stochastic star formation appears consistent with the value observed for nongiant H II regions but is larger than the value observed for giant H II regions. In the annulus where a global spiral pattern occurs in M33, the radial distribution of giant regions agrees with the steeper distribution predicted for a spiral density-wave model. These comparisons suggest that in M83 and M33, stochastic star formation and star formation by a spiral density wave both occur in the same galaxy. Stars in giant H II regions are likely to have formed as a result of a spiral density wave plus sequential star formation. The combination of sporadic and sequential star formation described in the stochastic models of Seiden and Gerola is more important for producing stars in nongiant H II regions.

Subject headings: galaxies: individual — nebulae: H II regions — stars: formation

I. INTRODUCTION

H II regions are among the best tracers of recent star formation in galaxies. It has long been recognized (see Baade 1963) that highly luminous H II regions are effective delineators of spiral structure. Two of the theories that have been proposed to account for the observed spiral patterns are the spiral density-wave theory of Lin and Shu (1964) and the stochastic star formation model of Gerola and Seiden (1978). We are interested (*i*) in using the spatial distribution of H II regions in galaxies to test these theories and (ii) in examining the spatial distributions of high and low luminosity H II regions separately to see if both involve the same star-forming mechanisms. The latter question is important because Mezger (1970) and Georgelin and Georgelin (1976) assert that giant H II regions are much better tracers of spiral structure than H II regions of lower luminosity.

To distinguish between giant and nongiant H II regions requires flux measurements, and to represent the global distribution of H II regions in a galaxy, one needs such data for a large number of H II regions. Although lists, photographs, and positions of H II regions have been published for many galaxies (see Hodge 1974) absolute flux measurements of a significantly large number of H II regions are presently available for only a few spiral galaxies (M33, M51, NGC 628 and our Galaxy). For M51 and NGC 628 only highly luminous H II regions have been measured (see Israel 1980 and Kennicutt and Hodge 1980). In this paper we provide positions, Hα flux measurements, and isophotal diameters for 296 H II regions in M83, a SAB(s)c, luminosity class I–II spiral galaxy. Thus we add to the small list of spiral galaxies for which a large sample of H II regions have been measured. Since the distance of M83 is 3.75 Mpc (de Vaucouleurs 1979), M83 is close enough so that not only giant H II regions but also H II regions of lower luminosity can be measured.

We have compiled our catalog of H II regions in M83 from the Hα surface photometry obtained by Talbot,

Jensen, and Dufour (1979). They have made their *UBVR* Hα maps available on computer tape to the astronomical community. From visual inspection of their plates, E. B. Jensen, R. J. Talbot, and R. J. Dufour (1981, private communication) noted that bright and faint H II regions are distributed differently in M83. Dividing the H II regions into subpopulations according to the value of the individual Hα flux (or, equivalently, excitation parameter U), we shall exhibit this quantitatively. We shall use our information on H II regions in M83, together with data on H II regions in M33 from Israel and van der Kruit (1974) and Boulesteix *et al.* (1974) to show that in each of these galaxies nongiant H II regions are less concentrated in a two-armed pattern and show a broader distribution as a function of galactocentric radius R than giant H II regions. We shall compare the observed radial distributions with the predictions of a stochastic star formation model and a spiral density-wave model and conclude that stochastic processes are more relevant for producing massive stars in nongiant H II regions. Obviously it would be important to know whether these results apply to a larger sample of spiral galaxies. The required data should be forthcoming from the large photometric survey that Hodge and Kennicutt are making of the H II region populations in 150 galaxies (see Kennicutt and Hodge 1980).

In § II, we present our catalog of H II regions in M83. In § III some of the physical properties of these H II regions are discussed. Luminosity and diameter distribution functions are presented, and are compared with those for other Sc galaxies in the literature. The azimuthal and radial distributions of H II regions in both M83 and M33 are shown in § IV; differences in the distributions for giant and nongiant regions are examined first qualitatively, and then quantitatively by means of various statistical tests. In § V we compare the observed radial distributions with those predicted by both the spiral density wave theory and by the stochastic star formation theory. Our results are discussed and interpreted in § VI, where we present some speculations as to the mechanisms governing star formation in these two galaxies. We summarize our conclusions in § VII.

II. H II REGIONS IN M83

We use the *UBVR* Hα surface photometry of M83 by Talbot, Jensen, and Dufour (1979) to compile a catalog of H II regions. As defined in Talbot *et al.*, and Talbot (1980), the pixel values F in their Hα map are on a linear surface brightness scale and are related to $I_{H\alpha}$, the Hα intensity in ergs cm^{-2} s^{-1} arcsec^{-2}, by

$$I_{H\alpha} = 1.66 \times 10^{-17} F. \quad (1)$$

The intensities are uncertain by ±5%.

Table 1 lists the catalog of H II regions we have compiled from their Hα and R maps of M83. R. J. Talbot (1979, private communication) notes that values of $F < 20$ are insignificant. To be conservative in isolating individual H II regions, we restrict consideration to pixels with $F > 100$. This choice should give a catalog that is reasonably complete to a specific lower intensity limit and reduces the possibility of confusion with the low-level diffuse Hα emission from the disk observed by Carranza (1968).

The H II regions in Table 1 are numbered in order of decreasing right ascension. Our coordinate system is based on the plate solution of Pennington, Talbot, and Dufour (1982). Pennington has kindly provided us with the α, δ coordinates of bootstrap standard stars. The second and third columns of Table 1 list the distance in the plane of the sky of each H II region from a reference point with coordinates $\alpha(1950.0) = 13^h34^m11^s.55 \pm 0^s.04$ and $\delta\ (1950.0) = -29°36'42''.2 \pm 0''.4$ (where the uncertainties are the formal errors in the plate solutions). The distances are in arcsec with the X coordinate increasing westward and the Y coordinate increasing northward. The pixel size in the maps of Talbot *et al.* is about 1''.48, and the values of X and Y in Table 1 are accurate to ±1''. The reference point is the pixel which Talbot *et al.* specify as approximately the nucleus and lies 5''.9 ± 0''.5 east and 7''.0 ± 0''.5 south of the radio position of peak intensity determined by Condon *et al.* (1982). The coordinate system of the Hα map on the computer tape which was supplied by Talbot, Jensen, and Dufour before doing a plate solution differs slightly in orientation from our coordinate system. Relative to the present system, this earlier map was rotated by 0°.67 ± 0°.05 counterclockwise. On request we can supply a listing of H II region positions in the coordinate system of this earlier map. The positions listed in the second and third columns are, for the most part, those of the centroid of each H II region. Exception was made for regions which exhibit obvious bright spots; for these, the position of peak intensity is given.

For each H II region, the sixth column lists the value of the integrated Hα flux $\mathscr{F}_{H\alpha}$ obtained simply by summing the values of F over the region. In the seventh column we give values for $\mathscr{F}_c$, the Hα flux corrected in an approximate fashion for extinction within the disk of M83 via the simplified model of Talbot (1980). The radial extinction gradient in the galaxy is estimated in Talbot's model from the gradients in the surface density of interstellar gas and the metal abundance; therefore, the corrections applied here are valid in a statistical sense only. Both $\mathscr{F}_{H\alpha}$ and $\mathscr{F}_c$ are in the photographic units of Talbot *et al.* Conversion of the corrected flux $\mathscr{F}_c$ to c.g.s. units is made in the eighth column, where the flux is listed as $S_{H\alpha}$ in ergs cm^{-2} s^{-1}. We adopt for M83 a distance D of 3.75 Mpc (de Vaucouleurs 1979), an inclination i to the line of sight of 24° and a position angle PA of the optical major axis of 45° (de Vaucouleurs, de Vaucouleurs, and Corwin 1976). For

TABLE 1

H II REGIONS IN M83

#	X	Y	R	Θ	F	F_c	log $S_{H\alpha}$	U	ρ	N_{GdV}
1	-345	139	6.87	25.0	768	941	-13.460	106	44	
2	-344	-231	8.22	79.8	1072	1242	-13.340	116	53	
3	-335	42	6.37	40.4	863	1082	-13.400	111	53	
4	-329	31	6.23	42.2	13574	17151	-12.200	279	91	
5	-325	273	7.72	5.5	454	537	-13.704	88	44	
6	-321	66	6.13	35.8	452	574	-13.675	90	44	
7	-294	256	7.08	4.3	755	916	-13.472	105	44	
8	-271	266	6.90	0.6	9686	11858	-12.360	246	97	
9	-269	57	5.14	35.3	279	376	-13.859	78	44	
10	-260	138	5.40	18.5	620	822	-13.519	101	44	
11	-248	92	4.88	26.7	3591	4927	-12.741	184	62	
12	-242	284	6.78	355.0	246	302	-13.954	72	44	
13	-241	205	5.76	5.0	14819	19248	-12.149	290	97	
14	-234	-1	4.47	47.8	425	600	-13.656	91	53	
15	-220	15	4.18	43.7	270	389	-13.844	79	44	
16	-222	-190	5.80	86.0	18389	23791	-12.057	311	119	
17	-217	2	4.13	47.0	530	768	-13.548	99	62	
18	-213	69	4.16	29.3	9261	13398	-12.307	257	75	
19	-211	-81	4.43	67.8	395	559	-13.686	89	53	
20	-211	-75	4.38	66.4	3833	5447	-12.698	190	115	60
21	-205	50	3.94	33.5	439	646	-13.624	93	62	
22	-200	59	3.86	30.8	3001	4446	-12.786	178	122	
23	-202	-193	5.57	88.8	398	522	-13.716	87	53	
24	-199	65	3.88	29.0	988	1462	-13.269	122	81	
25	-191	59	3.72	30.0	1018	1527	-13.250	124	53	
26	-190	70	3.74	26.7	1676	2509	-13.034	147	115	
27	-183	80	3.69	23.1	5485	8252	-12.517	218	144	59
28	-180	-117	4.26	78.9	6859	9843	-12.441	232	70	
29	-175	72	3.50	24.4	1908	2918	-12.969	154	102	
30	-169	-131	4.26	83.4	4249	6098	-12.649	197	162	
31	-161	25	3.07	38.8	2004	3190	-12.930	159	111	
32	-157	354	7.12	337.1	3684	4463	-12.784	178	62	
33	-159	18	3.02	41.0	3309	5289	-12.710	188	115	
34	-151	95	3.26	14.0	2835	4431	-12.787	177	133	
35	-149	53	2.92	27.5	5154	8325	-12.513	219	115	58
36	-148	26	2.82	37.4	462	753	-13.557	98	44	
37	-139	125	3.40	3.4	13086	20199	-12.129	294	193	57
38	-135	141	3.55	358.7	1604	2442	-13.046	145	86	
39	-136	23	2.59	38.0	362	605	-13.652	91	53	
40	-136	-221	5.13	102.3	3582	4831	-12.750	183	133	
41	-131	122	3.25	2.3	3040	4757	-12.757	182	97	
42	-129	288	5.80	337.3	228	295	-13.964	72	44	
43	-131	27	2.51	35.6	693	1169	-13.366	114	70	
44	-127	125	3.24	0.3	1129	1768	-13.186	130	70	
45	-130	-228	5.19	104.1	269	361	-13.876	77	44	
46	-122	130	3.23	358.0	1488	2332	-13.066	143	97	
47	-120	166	3.73	350.1	16721	25057	-12.035	316	231	56
48	-120	146	3.44	353.8	380	584	-13.667	90	53	
49	-122	-162	4.04	97.3	912	1332	-13.309	119	75	
50	-118	105	2.88	3.7	2105	3415	-12.900	163	91	
51	-117	-46	2.47	68.3	1122	1900	-13.155	134	75	
52	-116	-40	2.41	65.9	1352	2306	-13.071	143	91	
53	-115	46	2.28	25.3	958	1657	-13.215	128	62	
54	-114	150	3.43	351.4	783	1204	-13.353	115	70	
55	-115	27	2.20	34.3	30273	52890	-11.710	406	331	51, 54
56	-114	-28	2.28	61.2	1223	2115	-13.109	139	81	
57	-110	156	3.48	349.2	209	320	-13.929	74	44	
58	-109	172	3.72	346.1	901	1350	-13.304	119	62	
59	-110	55	2.25	20.1	15388	26726	-12.007	323	259	53
60	-110	-24	2.19	59.4	4500	7872	-12.538	215	148	
61	-107	165	3.59	346.8	230	349	-13.891	76	44	
62	-108	-14	2.09	54.6	3054	5399	-12.702	189	97	
63	-105	109	2.76	358.8	2431	3993	-12.833	171	97	
64	-109	-209	4.65	106.0	207	288	-13.974	71	44	
65	-102	86	2.42	5.0	235	400	-13.832	79	44	
66	-103	-33	2.11	64.8	18150	32031	-11.928	343	224	50
67	-99	187	3.89	341.4	410	606	-13.651	91	53	

TABLE 1—*Continued*

#	X	Y	R	Θ	F	F_c	log $S_{H\alpha}$	U	ρ	N_{GdV}
68	-99	164	3.51	344.9	8781	13417	-12.306	257	211	
69	-101	-5	1.93	50.1	6633	11957	-12.356	247	193	
70	-99	-16	1.94	56.5	19266	34688	-11.894	353	224	49,52
71	-99	-49	2.17	73.0	9705	16999	-12.203	278	215	
72	-97	21	1.85	35.5	371	675	-13.605	94	44	
73	-97	-59	2.24	77.7	12476	21678	-12.098	301	168	48
74	-93	187	3.84	339.7	558	828	-13.516	101	53	
75	-93	43	1.88	22.1	26936	48888	-11.745	395	281	46
76	-94	-163	3.73	103.8	1958	2934	-12.966	155	122	
77	-91	17	1.74	36.6	284	524	-13.715	87	44	
78	-92	-77	2.39	85.6	5466	9346	-12.463	228	141	47
79	-89	53	1.90	15.7	29895	54132	-11.700	409	288	46
80	-87	171	3.52	340.5	564	860	-13.499	102	62	
81	-85	165	3.41	340.8	991	1527	-13.250	124	75	
82	-86	62	1.93	10.2	1636	2950	-12.964	155	97	
83	-87	-58	2.08	79.4	3380	5988	-12.657	196	144	
84	-88	-133	3.17	100.6	468	737	-13.566	97	53	
85	-87	-143	3.32	102.6	645	1002	-13.433	108	70	
86	-82	141	2.98	344.0	15626	25079	-12.035	316	211	45
87	-83	29	1.63	28.1	6561	12300	-12.344	249	115	
88	-82	68	1.95	5.8	235	423	-13.808	81	44	
89	-85	-158	3.55	105.3	9296	14150	-12.283	261	219	
90	-80	196	3.90	335.3	628	927	-13.467	105	70	
91	-81	94	2.26	355.3	2514	4362	-12.794	176	119	
92	-79	152	3.15	341.0	3697	5838	-12.668	195	133	
93	-80	85	2.12	357.9	372	655	-13.618	94	53	
94	-79	-73	2.14	88.0	259	455	-13.776	83	44	
95	-76	65	1.81	4.6	743	1359	-13.301	119	62	
96	-74	175	3.49	336.0	786	1202	-13.354	115	81	
97	-77	-176	3.78	109.7	254	379	-13.855	78	44	
98	-73	77	1.93	358.4	364	656	-13.617	94	53	
99	-71	65	1.75	3.0	216	398	-13.834	79	44	
100	-72	-89	2.27	95.5	234	405	-13.826	80	44	
101	-67	72	1.79	358.0	1172	2152	-13.101	139	86	
102	-69	-186	3.89	112.6	981	1450	-13.272	122	81	
103	-65	59	1.59	3.0	511	962	-13.451	106	53	
104	-67	-108	2.51	102.0	7867	13273	-12.311	256	179	44
105	-61	158	3.13	334.2	1425	2254	-13.081	141	97	
106	-60	216	4.17	328.3	6756	9759	-12.444	231	159	
107	-60	167	3.27	332.7	284	443	-13.787	82	44	
108	-58	-120	2.61	107.8	419	698	-13.590	96	53	
109	-53	150	2.95	332.4	24471	39421	-11.838	368	233	43
110	-51	58	1.41	356.0	42557	82092	-11.520	470	286	42
111	-48	138	2.71	332.1	2340	3861	-12.847	169	126	
112	-50	-130	2.74	112.2	905	1489	-13.261	123	86	
113	-45	156	3.02	328.9	493	788	-13.537	100	44	
114	-42	95	1.91	337.0	449	811	-13.525	100	62	
115	-45	-123	2.57	113.1	903	1513	-13.254	124	86	
116	-45	-213	4.22	120.7	9895	14238	-12.280	262	197	
117	-41	-51	1.29	95.6	261	512	-13.725	86	44	
118	-35	55	1.19	346.0	22938	45663	-11.774	387	257	41
119	-33	47	1.05	349.0	357	725	-13.574	97	53	
120	-35	-125	2.52	117.1	11434	19251	-12.149	290	164	40
121	-34	-152	3.03	120.1	226	361	-13.876	77	44	
122	-30	134	2.57	325.1	24468	40982	-11.821	373	262	39
123	-28	197	3.75	320.7	448	670	-13.608	94	44	
124	-31	-72	1.55	109.8	342	647	-13.623	93	44	
125	-30	66	1.33	337.3	14896	29057	-11.971	332	231	38
126	-32	-144	2.86	120.1	7279	11825	-12.361	246	219	
127	-25	115	2.20	324.6	2406	4199	-12.811	174	106	
128	-24	-141	2.76	123.1	447	733	-13.569	97	62	
129	-22	-70	1.43	115.4	3597	6924	-12.593	206	111	37
130	-21	-152	2.96	124.8	1362	2190	-13.093	140	102	
131	-16	36	0.72	337.3	6255	13390	-12.307	257	197	
132	-15	87	1.66	321.9	277	516	-13.721	86	44	
133	-15	-57	1.14	118.2	252	505	-13.731	86	44	
134	-16	-136	2.64	125.8	233	387	-13.846	78	44	

TABLE 1—*Continued*

#	X	Y	R	Θ	F	F_c	log $S_{H\alpha}$	U	ρ	N_{GdV}
135	-17	-214	4.12	127.9	13937	20213	-12.128	295	219	36
136	-13	-141	2.73	127.2	448	738	-13.566	97	62	
137	-8	30	0.57	328.1	38062	83442	-11.512	473	230	35
138	-5	-45	0.87	126.3	1186	2477	-13.040	146	75	
139	-4	25	0.48	320.8	3037	6767	-12.603	204	86	
140	-6	-138	2.63	130.1	249	414	-13.817	80	44	
141	-4	-57	1.09	128.2	457	923	-13.469	105	53	
142	-5	-149	2.86	130.5	2419	3931	-12.839	170	137	
143	2	-161	3.07	133.0	331	526	-13.713	87	53	
144	2	-142	2.70	133.4	12951	21397	-12.103	300	202	34
145	8	235	4.49	310.6	260	366	-13.870	77	44	
146	13	195	3.75	308.5	14757	22066	-12.090	303	221	30,32
147	10	-66	1.25	141.2	1568	3095	-12.943	157	115	
148	12	-220	4.17	135.4	1543	2228	-13.086	141	106	
149	13	-148	2.81	137.6	508	829	-13.515	101	62	
150	13	-176	3.34	136.7	417	646	-13.624	93	44	
151	18	41	0.88	288.9	1087	2269	-13.078	142	75	
152	20	-149	2.83	140.1	12184	19858	-12.136	293	206	29
153	22	-64	1.25	152.0	1530	3020	-12.954	156	97	
154	27	230	4.45	305.9	5850	8269	-12.516	218	137	27
155	23	-58	1.16	154.8	359	717	-13.578	96	53	
156	26	103	2.07	298.7	674	1195	-13.356	114	75	
157	28	213	4.15	305.1	6886	9962	-12.435	233	170	26
158	28	-65	1.30	156.5	1020	1998	-13.133	136	75	
159	32	-4	0.61	220.4	1197	2611	-13.017	149	86	
160	34	-57	1.22	164.2	1195	2369	-13.059	144	81	
161	37	92	1.95	291.3	370	665	-13.611	94	44	
162	34	-122	2.36	148.2	232	397	-13.835	79	44	
163	40	300	5.83	304.9	2066	2667	-13.008	150	106	
164	36	-65	1.36	162.1	513	996	-13.436	108	62	
165	37	-115	2.23	150.8	511	888	-13.485	104	62	
166	43	77	1.75	284.3	317	584	-13.667	90	53	
167	45	116	2.45	291.8	1777	3015	-12.955	156	106	
168	44	-49	1.20	176.4	2983	5929	-12.661	196	119	
169	47	93	2.06	286.6	245	434	-13.796	81	44	
170	48	122	2.57	291.8	717	1200	-13.355	115	62	
171	51	242	4.79	300.8	481	663	-13.612	94	62	
172	48	1	0.92	228.8	1401	2906	-12.971	154	81	
173	51	227	4.52	300.0	1430	2010	-13.131	136	86	
174	49	7	0.95	235.2	474	978	-13.444	107	53	
175	50	102	2.25	287.2	258	448	-13.783	82	44	
176	46	-171	3.30	147.9	3354	5215	-12.717	187	126	
177	49	-166	3.22	149.1	252	395	-13.837	79	44	
178	49	-153	2.98	150.7	357	572	-13.676	89	53	
179	55	134	2.84	291.1	561	913	-13.473	105	70	
180	56	110	2.44	286.8	213	362	-13.875	77	44	
181	57	141	2.99	291.2	4020	6444	-12.625	201	141	
182	56	-53	1.40	182.1	7849	15157	-12.253	268	179	25
183	56	-71	1.64	172.8	831	1553	-13.243	125	62	
184	59	80	1.97	277.9	1919	3443	-12.897	163	122	
185	64	125	2.77	286.4	24167	39626	-11.836	369	293	24
186	64	114	2.58	284.1	1458	2439	-13.047	145	102	
187	64	-61	1.60	181.6	1190	2238	-13.084	141	86	
188	70	215	4.41	295.0	571	809	-13.526	100	70	
189	68	69	1.93	270.2	8220	14828	-12.263	266	202	
190	67	-66	1.71	180.7	530	982	-13.442	107	53	
191	66	-137	2.79	159.3	5385	8804	-12.489	223	170	
192	69	-103	2.26	167.9	771	1336	-13.308	119	53	
193	75	224	4.62	294.5	589	822	-13.519	101	44	
194	74	100	2.46	277.9	2075	3517	-12.888	164	119	
195	74	88	2.27	274.6	3152	5459	-12.697	190	122	
196	75	-19	1.44	213.3	981	1884	-13.159	133	70	
197	84	86	2.39	270.5	13079	22360	-12.084	305	235	21
198	84	72	2.21	266.1	27013	47151	-11.760	391	288	20
199	89	175	3.87	286.7	527	780	-13.542	99	53	
200	88	52	2.03	257.0	6736	12010	-12.354	248	157	
201	90	187	4.09	287.8	10695	15550	-12.242	270	157	19

TABLE 1—*Continued*

#	X	Y	R	Θ	F	F_c	log $S_{H\alpha}$	U	ρ	N_{GdV}
202	92	205	4.43	289.2	2174	3079	-12.945	157	91	
203	91	-43	1.86	201.6	219	398	-13.834	79	44	
204	94	44	2.05	251.8	6062	10780	-12.401	239	153	17
205	92	-123	2.79	170.9	332	542	-13.700	88	44	
206	93	-93	2.40	179.9	1036	1766	-13.187	130	81	
207	99	214	4.64	288.7	808	1126	-13.382	112	70	
208	97	-16	1.85	218.3	454	827	-13.516	101	44	
209	100	26	2.00	241.7	44210	79076	-11.536	464	321	16
210	100	-31	1.94	209.8	719	1294	-13.322	118	62	
211	103	48	2.24	251.5	27615	48023	-11.752	393	275	14
212	103	-22	1.96	215.2	466	837	-13.511	102	53	
213	106	11	2.04	233.4	60548	107789	-11.401	515	371	12
214	111	60	2.49	254.6	1962	3317	-12.913	161	119	
215	113	36	2.33	244.7	7154	12319	-12.343	250	170	
216	118	61	2.63	253.9	539	897	-13.481	104	70	
217	118	-19	2.25	218.1	1518	2636	-13.013	149	91	
218	121	99	3.11	264.9	321	509	-13.727	86	44	
219	119	-53	2.41	202.7	222	378	-13.856	78	44	
220	118	-131	3.21	176.8	7342	11510	-12.373	244	179	
221	124	108	3.27	266.4	9701	15155	-12.253	267	175	7
222	121	-123	3.13	179.5	617	974	-13.445	107	70	
223	124	79	2.92	258.5	42817	69230	-11.594	444	386	6
224	126	101	3.21	264.2	317	497	-13.737	85	53	
225	125	13	2.42	233.2	465	792	-13.535	100	62	
226	124	-159	3.67	172.4	291	437	-13.793	82	44	
227	124	-173	3.87	169.8	698	1031	-13.421	109	81	
228	127	-30	2.44	214.2	3431	5828	-12.668	194	159	
229	129	29	2.56	239.8	3900	6542	-12.618	202	75	5
230	129	-3	2.46	226.2	6513	11049	-12.391	241	175	
231	130	17	2.53	234.8	1010	1700	-13.203	129	81	
232	128	-123	3.23	181.1	258	403	-13.829	79	44	
233	130	-43	2.54	208.7	21107	35464	-11.884	355	310	
234	130	-128	3.32	180.4	1498	2323	-13.068	143	102	
235	131	-118	3.20	183.3	214	335	-13.909	75	44	
236	139	-17	2.63	220.7	11899	19804	-12.137	292	262	
237	142	22	2.78	236.2	3328	5457	-12.697	190	157	
238	141	-65	2.85	201.9	532	864	-13.497	103	62	
239	143	38	2.88	242.1	3379	5482	-12.695	190	111	4
240	143	15	2.77	233.4	343	563	-13.683	89	53	
241	144	-28	2.74	216.3	531	873	-13.493	103	70	
242	146	-37	2.81	213.3	1811	2955	-12.963	155	115	
243	149	89	3.43	257.0	314	483	-13.750	84	53	
244	149	60	3.15	248.6	1243	1963	-13.141	135	97	
245	155	-28	2.96	217.4	3368	5416	-12.700	190	153	
246	162	-46	3.12	211.3	291	460	-13.771	83	53	
247	167	34	3.31	238.8	4443	6916	-12.594	206	150	
248	168	-15	3.19	222.6	467	734	-13.568	97	62	
249	173	-13	3.28	223.3	349	544	-13.698	88	53	
250	190	-102	3.96	198.4	251	368	-13.868	77	44	
251	192	-52	3.70	212.2	566	849	-13.505	102	70	
252	193	-41	3.69	215.5	3613	5429	-12.699	190	141	
253	196	81	4.16	249.4	712	1030	-13.421	109	53	
254	195	-86	3.92	202.9	325	478	-13.754	84	53	
255	202	83	4.29	249.0	212	303	-13.952	72	44	
256	201	-86	4.02	203.7	506	738	-13.566	97	62	
257	203	-47	3.89	214.2	1226	1811	-13.176	132	91	
258	208	84	4.41	248.7	310	439	-13.791	82	44	
259	206	-43	3.94	215.8	453	666	-13.610	94	44	
260	207	-81	4.10	205.7	481	697	-13.591	96	62	
261	210	-46	4.02	215.0	357	521	-13.717	87	53	
262	211	-147	4.70	191.1	524	726	-13.573	97	44	
263	217	34	4.24	236.3	1492	2145	-13.102	139	102	
264	218	-33	4.14	218.9	1276	1848	-13.167	132	102	
265	221	-66	4.28	210.5	231	330	-13.915	74	44	
266	225	-25	4.28	221.3	13896	19910	-12.135	293	206	3
267	228	-36	4.33	218.6	545	777	-13.543	99	53	
268	230	-9	4.38	225.5	493	701	-13.588	96	62	

TABLE 1—*Continued*

#	X	Y	R	Θ	F	F_c	log $S_{H\alpha}$	U	ρ	N_{GdV}
269	233	-31	4.42	219.9	347	491	-13.743	85	53	
270	238	40	4.67	237.0	491	683	-13.599	95	62	
271	239	-22	4.54	222.3	227	318	-13.931	73	44	
272	241	-32	4.57	219.9	2491	3491	-12.891	164	115	
273	252	-25	4.78	222.0	1952	2695	-13.003	150	115	
274	255	2	4.87	228.1	1331	1827	-13.172	132	86	
275	265	38	5.16	235.6	8462	11394	-12.377	243	162	1
276	286	103	5.96	246.7	695	892	-13.483	104	53	
277	295	-1	5.61	227.3	279	365	-13.872	77	44	
278	296	-35	5.63	220.8	370	483	-13.750	84	53	
279	337	331	9.40	269.6	422	472	-13.760	84	44	
280	332	-209	7.17	194.0	500	602	-13.654	91	44	
281	342	5	6.53	228.3	547	680	-13.601	95	44	
282	354	304	9.28	266.0	3501	3935	-12.839	170	62	
283	357	-104	6.91	210.9	247	301	-13.955	72	44	
284	381	-59	7.25	218.7	490	589	-13.664	90	62	
285	77	-71	1.90	182.8	35549	64304	-11.626	433	191	22
286	82	-75	2.02	183.0	2580	4600	-12.771	180	91	
287	92	-72	2.13	187.6	16768	29494	-11.964	334	170	18
288	106	-79	2.40	189.2	17565	29959	-11.957	336	197	11
289	97	-61	2.09	194.2	14047	24817	-12.039	315	153	15
290	103	-52	2.11	200.0	23262	41004	-11.821	373	179	13
291	107	-66	2.29	194.5	13827	23873	-12.056	311	168	10
292	119	-62	2.47	198.9	5546	9386	-12.461	228	119	8
293	78	-68	1.88	184.3	16683	30261	-11.953	337	264	
294	101	-72	2.25	190.4	54094	93818	-11.462	492	513	
295	122	-62	2.52	199.6	11121	18724	-12.161	287	268	
296	111	-43	2.19	205.7	36988	64600	-11.624	434	410	

NOTE.— X and Y are in arcsec in the plane of the sky; R is in kpc and θ in degrees in the plane of the Galaxy; the units of $S_{H\alpha}$ are ergs cm^{-2} s^{-1}; the units of U are pc cm^{-2}; and the units of ρ are pc.

these values the fourth and fifth columns of Table 1 give positions in the plane of M83 with R, the distance from the center in kpc, and θ, the angle measured eastward from the northeastern line of nodes. We use expressions given in Peimbert, Rayo, and Torres-Peimbert (1975) and Mezger and Henderson (1967) to relate the Hα and free-free intensities and thus calculate the values for the excitation parameter U listed in the ninth column. The values of U include the statistical correction for extinction and are based on an assumed electron temperature T_e of 10^4 K. Since U is a measure of the total Lyman continuum flux, it is useful as an index of the distribution of O stars in the galaxy. The qualitative results of § IV, where we compare the spatial distributions of low and high excitation H II regions in the plane of M83, are not very sensitive to the assumed values of D, i, PA, or T_e.

For each H II region the tenth column of Table 1 lists values in pc for the average linear diameter $\rho = \theta D$ in the plane of the sky. We define the average angular diameter (characteristic dimension) θ of an H II region to be $2(\Delta\Omega/\pi)^{1/2}$, where $\Delta\Omega$ is the solid angle subtended. The pixel size, 1".48, in the maps of Talbot *et al.* is comparable to their estimate for the seeing limit of their Hα plate. This gives the uncertainty in the values of ρ. We note that at the distance of M83, 1" equals 18 pc, and thus classical H II regions with $\rho < 30$ pc would be unresolvable. Many of the large H II complexes with irregular boundaries were divided into individual regions corresponding to separate bright spots. In some cases the basis for division is somewhat arbitrary; in particular, the large complex at the SW extremity of the bar was divided into eight "hot spots" (regions 285–292 in Table 1) and four large regions of lower intensity (293–296).

After this work was completed, we received a preprint from de Vaucouleurs, Pence, and Davoust (1983), in which they have also used the maps of Talbot *et al.* to compile a catalog of the 60 brightest H II regions in M83. For reference, we list the catalog numbers for most of the regions in their list in the eleventh column of Table 1.

III. LUMINOSITY FUNCTION AND SIZE DISTRIBUTION FUNCTION FOR H II REGIONS IN M83

In this section we discuss the luminosity and size distributions among the H II regions in M83.

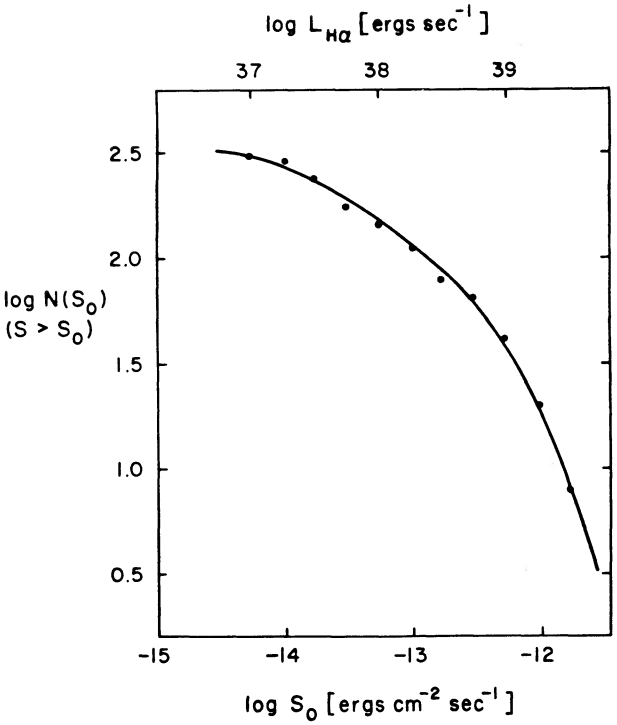

FIG. 1.—The integrated number of H II regions $N(S_0)$ in M83 with Hα flux $S_{H\alpha} > S_0$. The high-luminosity ($\mathscr{L}_{H\alpha} > 4\times10^{38}$ ergs s^{-1}) portion of this integrated luminosity function approximates a power law with index $\beta = 1.4 \pm 0.2$.

In Figure 1 we plot, on a double logarithmic scale, the integrated number $N(S_0)$ of H II regions with Hα fluxes $S_{H\alpha} > S_0$. Because the catalog in Table 1 is assumed to be complete at least down to $\log S_{H\alpha} \approx -13.5$ in c.g.s. units, the curvature of the relation in Figure 1 is probably real and not due entirely to incomplete sampling. The integrated luminosity function is not well represented by a single power law, in contrast to the luminosity functions determined for two other Sc galaxies: M33 (Israel and van der Kruit 1974) and NGC 628 (Kennicutt and Hodge 1980). However, most of the H II regions in our catalog for M83 have luminosities $\mathscr{L}_{H\alpha}$ below the detection limit for H II regions in NGC 628. If only highly luminous regions with $U > 200$ pc cm^{-2} ($\mathscr{L}_{H\alpha} > 10^{38.6}$ ergs s^{-1}) in M83 are considered, then a power law of the form $N(S_0) \propto S_0^{-\beta}$, with $\beta = 1.4 \pm 0.2$ does give a good fit. This is in good agreement with the value of $\beta = 1.5 \pm 0.2$ which Kennicutt and Hodge obtain for H II regions with $\mathscr{L}_{H\alpha} > 10^{38.5}$ ergs s^{-1} in NGC 628. From radio observations of 14 late-type galaxies, Israel (1980) finds that in most of these galaxies, the luminosity function for the H II region population follows a power law with $\beta = 1.75 \pm 0.5$. However, only for the galaxies M33, M51, LMC, and SMC does he have data on at least 15 H II regions per galaxy. Also, except in the galaxies M33, SMC, and LMC, his H II regions are large complexes with $U > 300$ pc cm^{-2}. Therefore, as Israel notes, it is possible that the single power-law approximation applies only to very bright H II regions. For M83, we find that while the high luminosity portion of the luminosity function can be characterized as a power law, the luminosity function does, indeed, level off for $U < 200$ pc cm^{-2}.

The total Hα flux from all of the H II regions listed in Table 1 is 9.2×10^{-11} ergs cm^{-2} s^{-1}. This is only 50% of the total Hα emission from M83, estimated at 1.8×10^{-10} ergs cm^{-2} s^{-1} (Talbot 1980). Since extrapolation of the luminosity function in Figure 1 to low fluxes may not be valid, it is unclear how much of the remaining 50% emanates from a population of faint, undetected H II regions, and how much is due to the background disk emission.

The number $N(\rho)d\rho$ of H II regions in M83 with diameters in an interval $d\rho$ about ρ is shown in Figure 2. We exclude here regions with $\rho < 60$ pc, since these are certainly undersampled (i.e., an H II region with $\rho = 44$ pc has only 2 pixels above our isophotal limit of 1.66×10^{-15} ergs cm^{-2} s^{-1} $arcsec^{-2}$). The diameter distribution function follows a power law $N(\rho) \propto \rho^{-\alpha}$ with $\alpha = 2.6 \pm 0.3$. This is smaller than the average value of $\alpha \approx 4$ that Kennicutt and Hodge (1980) find for the Sc galaxies M33, NGC 628, NGC 2403, and NGC 3631. If we restrict to regions in M83 with $\rho > 150$ pc (in effect, restricting to highly luminous regions), then $\alpha = 3.2 \pm 0.6$. Our diameters are isophotal, whereas the diameters in the distribution functions shown by Kennicutt and Hodge were eye-estimates.

By assuming that all Sc-Ir galaxies have the same diameter distribution function as NGC 628, Kennicutt

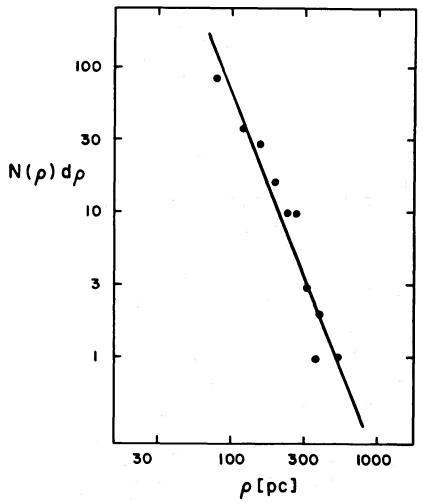

FIG. 2.—Diameter distribution function for H II regions in M83. The solid line, which is the best fitting power law to the entire distribution, has index $\alpha = 2.6 \pm 0.3$.

and Hodge derived the observed ($\log \langle \rho \rangle_3$, M_{pg}^0) relation between the average diameter of the three largest H II regions and the absolute magnitude of the parent galaxy. If, instead, one substitutes into their derivation the value of the power law index $\alpha = 3.2 \pm 0.6$ obtained for isophotal diameters of *large* H II regions in M83, then the predicted slope of the ($\log \langle \rho \rangle_3$, M_{pg}^0) relation $= -0.18^{+0.07}_{-0.04}$. With isophotal diameters for the Sandage-Tammann (1974) sample of galaxies, Kennicutt (1979) found an observed slope of -0.148 for the ($\log \langle \rho \rangle_3$, M_{pg}^0) relation. Thus, provided we consider only regions with $\rho > 150$ pc, our data on M83 is consistent with their interpretation of the ($\log \langle \rho \rangle_3$, M_{pg}^0) relation. The three largest isolated regions in M83, numbers 223, 213, and 55, respectively, have $\langle \rho \rangle_3 = 363$ pc.

Note that in both the luminosity and the diameter distribution functions, there is a qualitative difference between high and low luminosity regions. This suggests that the H II regions in M83 are composed of two populations, perhaps formed by different mechanisms.

The rms electron density n_e (rms) was calculated for each H II region from its diameter and excitation parameter by assuming a uniform sphere. Classical H II regions with $\rho < 30$ pc would be unresolved. The values of n_e (rms) range from 3 to 20 cm^{-3} and are plotted in Figure 3 as a function of ρ. The values of n_e (rms) and ρ are generally typical of Class V H II regions in the classification scheme of Habing and Israel (1979). As is usual, the measurements by Dufour *et al.* (1980) of [O III] and [S II] line strengths in five H II regions in M83 indicate much higher electron densities ($n_e =$ 200–500 cm^{-3}) and, thus, a filamentary structure. Their H II regions I, II, III, V, and VI correspond to numbers 137, 110, 213, 266, and 275, respectively, in our catalog. In Table 2 we list average values of n_e (rms) for subpopulations of H II regions grouped according to excitation parameter. We see that the values of n_e (rms) show considerable scatter and no clear trend as a function of U.

Are the giant ($U > 115$ pc cm^{-2}) H II regions single objects, containing multiple star systems, or is each giant region a collection of small discrete regions associated with separate clouds? We can address this question, at least in a statistical sense, by plotting the excitation parameter U as a function of diameter ρ (Fig. 4). If the giant H II regions are in fact single objects, then we would expect a linear relation between U and ρ, since Table 2 indicates there is no systematic trend in n_e (rms) with increasing U. A collection of separate Strömgren spheres, on the other hand, would give a larger diameter for a given value of U, unless they happened to be aligned along our line of sight. Since we see M83 nearly face-on, alignment of several spheres along our line of sight is less likely. If each giant H II region were composed of a collection of separate Strömgren spheres forming a two-dimensional distribution in the plane of the galaxy with no overlapping, we would expect to see a relation in Figure 4 of the form $U \propto \rho^{\gamma}$ with $\gamma \leq 2/3$ (if we allow for some space between the separate spheres). Although there is a significant amount of scatter in Figure 4, there is no evidence for a relation of this form. We conclude that the average giant H II region in

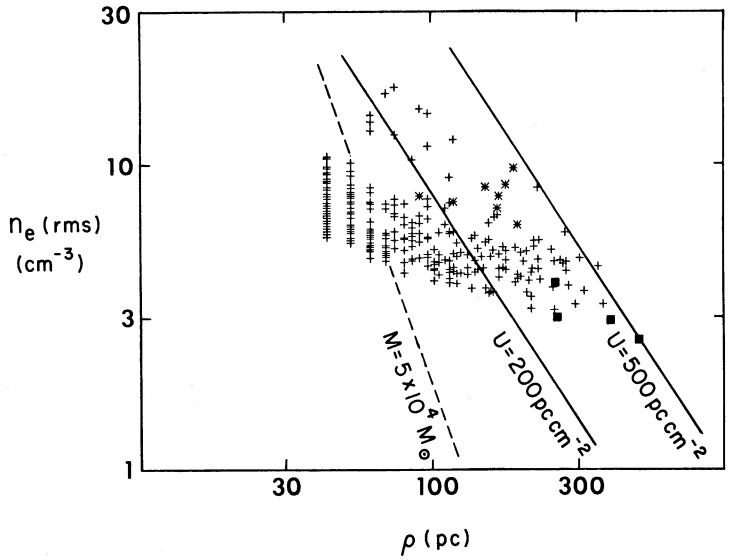

FIG. 3.—The rms electron densities of resolved H II regions in M83 plotted as a function of average diameter ρ. The solid lines are lines of constant excitation parameter; the dashed line is one of constant mass. H II regions in the large emission complex at the southwest extremity of the bar (see § II) are denoted by distinctive symbols: the eight "hot spots" (regions 285–292) by asterisks and the four large regions (regions 301–304) of lower-intensity diffuse emission by boxes.

TABLE 2

n_e (rms) FOR H II REGIONS IN M83 GROUPED ACCORDING TO EXCITATION PARAMETER

U (pc cm^{-2})	n_e (rms) (cm^{-3})
<115	6.78 ± 1.30
115–150	6.09 ± 1.49
150–200	5.86 ± 2.46
> 200	6.05 ± 3.08

M83 represents a single object, excited by multiple OB stars, and attribute most of the scatter in Figures 3 and 4 to scatter in the rms electron densities.

Finally, we comment on the question of whether the H II regions are mainly radiation or mainly density bounded. A good deal of controversy has arisen over this issue, and it is possible that the average giant H II region is radiation bounded in some directions and density bounded in others (see Lada, Blitz, and Elmegreen 1978). For M33, Israel and van der Kruit (1974) plot n_e (rms) versus ρ and find that the upper boundary to the observed distribution is a line of constant U; they conclude that the luminous H II regions in M33 are radiation bounded. Comte and Monnet (1974), however, observe that the brightest H II regions in M33 appear to blend into the diffuse Hα emission from the disk. They attribute this interarm emission to leakage of Ly-continuum photons from the luminous H II regions, and conclude that these regions must be density bounded!

The solid lines in Figure 3 are lines of constant excitation parameter ($n_e^2 D^3$ = constant), while the dashed line is a line of constant mass ($n_e D^3$ = constant). The distribution appears to be bounded by the line $U = 500$ pc cm^{-2}; this suggests that the most luminous H II regions in M83 may be radiation bounded.

In Figure 5 we show a contour plot of several highly luminous ($U > 200$ pc cm^{-2}) regions along the western arm. Most of these have obvious small bright cores, consistent with single objects that are mainly radiation bounded and excited by multiple O stars. This plot includes region number 213, the single H II region with the largest Hα flux in M83.

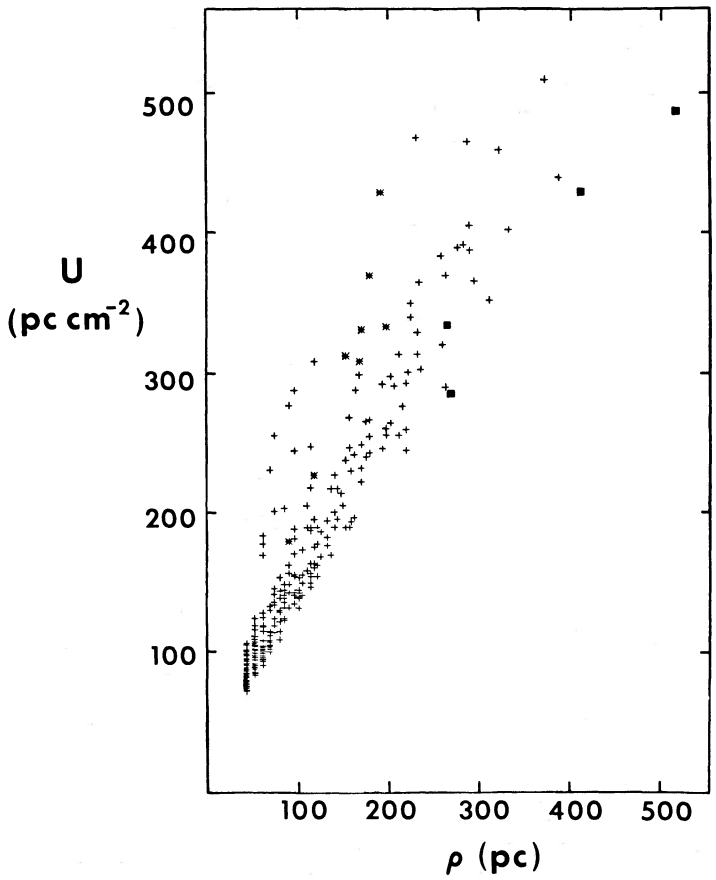

FIG. 4.—Excitation parameter vs. diameter for resolved H II regions in M83. The symbols have the same meaning as in Fig. 3.

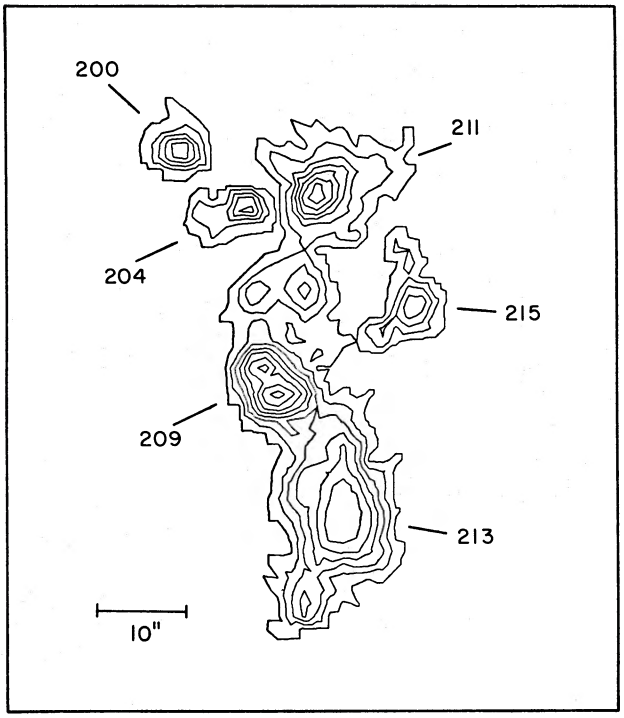

FIG. 5.—An isophotal Hα map of a group of six highly luminous H II regions along the western arm. The intensity scale is logarithmic; the contour interval equals 0.5 mag, and the lowest contour level corresponds to intensity $I_{H\alpha}=1.9\times10^{-15}$ ergs s^{-1} cm^{-2} $arcsec^{-2}$.

IV. DISTRIBUTION OF H II REGIONS IN M83 AND M33

In this section we study the radial and azimuthal distributions of H II regions in M83 and M33. Since values for the excitation parameters of individual H II regions are available for these two galaxies, we can compare the distribution of giant H II regions in the plane of each galaxy with the distribution of nongiant H II regions. According to Baade (1963), highly luminous H II regions are often "strung out like pearls along the arms" in spiral galaxies. Mezger (1970) and Georgelin and Georgelin (1976) consider giant H II regions to be better tracers of spiral structure than low-excitation H II regions. We first show that this is in fact the case in both M83 and M33: the giant H II regions are more concentrated in a two-armed pattern than the nongiant H II regions. We then find that giant and nongiant H II regions also differ in their radial distributions.

The distribution of H II regions in the plane of M83 is presented in Figure 6, where we divide H II regions into groups according to excitation parameter U. Recall that Mezger (1970) defines giant H II regions as those with $U>100$ pc cm^{-2}. Here we choose $U=115$ pc cm^{-2} as the dividing line because published values of U for M33 are available only for regions with $U>115$ pc cm^{-2}. The maps in Figure 6 are oriented with the X-axis parallel to the line of nodes. In Figure 6*a* we plot H II regions in M83 with $U<115$ pc cm^{-2}. It takes some imagination to see a two-armed spiral pattern in this distribution of low-excitation regions. In Figure 6*b* we plot H II regions with $U>115$ pc cm^{-2}, and in Figure 6*c* we restrict consideration to those regions with $U>150$ pc cm^{-2}. It is apparent that as we restrict our plots to regions of higher excitation parameter, the two-armed spiral pattern becomes better defined.

We define a "contrast factor" $\mathcal{R}$ as the ratio of the surface number density of H II regions inside the spiral arms to the surface density outside the arms: $\mathcal{R}=N_{in}/N_{out}$. Using Hα isophotes, we consider two possible choices for an observational definition of the spiral arms. The first (shown in Fig. 7) retains the observed asymmetry, while in the second we adopt a symmetric system which replaces the NE arm with a reflection of the SW arm. In both cases the arm widths are approximately constant over their total extent; we find arm widths (to 10% peak intensity) of 650 pc for the asymmetric arm system and 600 pc for the symmetric system. We compare with the values for the arm width in arc sec obtained by others for M83: from blue plates Block (1982) finds about the same value as we do, while Kennicutt (1982) finds smaller widths for the Hα arms by using a different criterion for defining arm widths. In calculating $\mathcal{R}$, we restrict consideration to the range of galactocentric distance 0.5–5.0 kpc and thus avoid the bright central nucleus.

Table 3 shows that the value of the contrast ratio $\mathcal{R}$ is significantly larger for regions with $U>200$ pc cm^{-2} than for regions with $U<115$ pc cm^{-2} and that there is some tendency for $\mathcal{R}$ to increase as regions with smaller values of U are progressively excluded from the sample. The quoted errors in $\mathcal{R}$ are counting errors involving regions near the adopted spiral arm boundaries (typically within ~ 60 pc), and n is the total number of H II regions in each sample; the smallest measured value of U in our sample is approximately 70 pc cm^{-2}. The results quantify the visual impression conveyed by Figure 6.

We also considered a third choice for the spiral arms, i.e., a logarithmic spiral pattern with a pitch angle of 14° and an arm width of 700 pc. While this again showed that the value of $\mathcal{R}$ increases as U increases, the 14° spiral does not fit the observed arm system well at all positions. Kennicutt (1981) also finds that in most spiral galaxies the arms deviate significantly from purely logarithmic or hyperbolic forms.

For M33, we make a similar comparison between the azimuthal distributions of giant and nongiant H II regions. Again we find that the two-armed pattern is better defined by the giant regions (see Fig. 8). We employ the list of giant radio H II regions in Israel and van der Kruit (1974), and the tabulation of Hα sources

by Boulesteix *et al.* (1974). For M33 we use $D = 0.72$ Mpc, $i = 55°$, and PA $= 23°$ (de Vaucouleurs 1959, 1978). Israel and van der Kruit measure continuum fluxes at 1415 MHz for individual radio sources that coincide with Hα sources in Boulesteix *et al.* (1974) and have values of U greater than 115 pc cm^{-2}; Boulesteix *et al.* (1974) did not measure the Hα fluxes for individual H II regions. We assume that those Hα sources not coinciding with radio sources listed in Israel and van der Kruit (1974) are of low excitation. The distributions of these low-excitation ($U < 115$ pc cm^{-2}) regions in the plane of M33 is shown in Figure 8*a*. Note that one sees a number of spiral-like features, rather than a dominant two-armed pattern. H II regions with $U > 115$ pc cm^{-2} are plotted in Figure 8*b*; although the spiral arm system is not as clearly defined in this galaxy as it is in M83, the two major arms can be discerned. Thus it appears that in this galaxy as well, the giant and nongiant H II regions are distributed differently in azimuth, and that the two-armed spiral shows up more clearly in the distribution of giant H II regions.

We next consider the radial distributions in each galaxy. Figure 9 shows, for M83, the surface densities of giant and nongiant H II regions as a function of galactocentric radius R. The distribution for regions with $U > 115$ pc cm^{-2} exhibits a sharp peak at a distance of $R = R_{\rm peak} \approx 2.3$ kpc, whereas the distribution function for the low-excitation regions appears to be broader and flatter. Figure 10 shows the radial distributions for M33. We see that in M33, also, the nongiant H II regions have a broader radial distribution in the galaxy than do the giant regions.

Before proceeding to statistical tests of these differences, we comment on how systematic errors in the assumed extinction gradients could influence our results. Extinction may cause two problems: (*i*) failure to detect

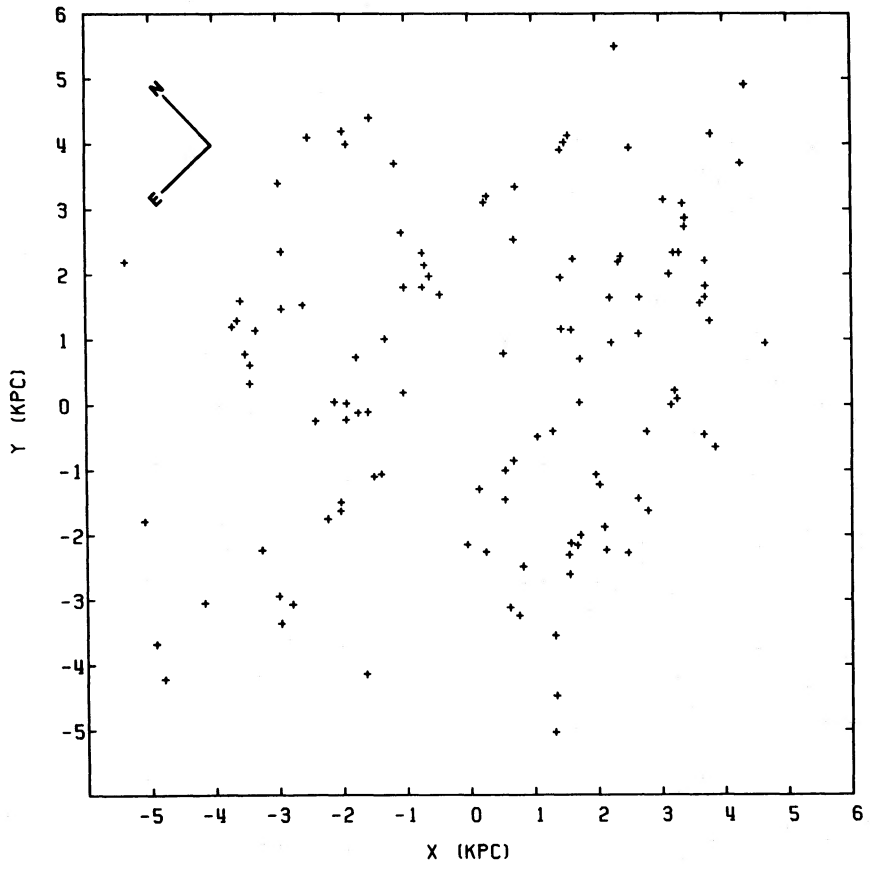

FIG. 6*a*

FIG. 6.—(*a*) The distribution of nongiant H II regions ($U < 115$ pc cm^{-2}) in the plane of M83. (*b*) The distribution of giant H II regions ($U > 115$ pc cm^{-2}) in the plane of M83. Crosses correspond to regions with $U = 115$–150 pc cm^{-2}; x's to regions with $U = 150$–200 pc cm^{-2}, and diamonds to regions with $U > 200$ pc cm^{-2}. (*c*) The distribution of H II regions with $U > 150$ pc cm^{-2} in the plane of M83. Crosses correspond to regions with $U = 150$–200 pc cm^{-2}, x's to regions with $U = 200$–230 cm^{-2}, and diamonds to supergiant regions with $U > 230$ pc cm^{-2}.

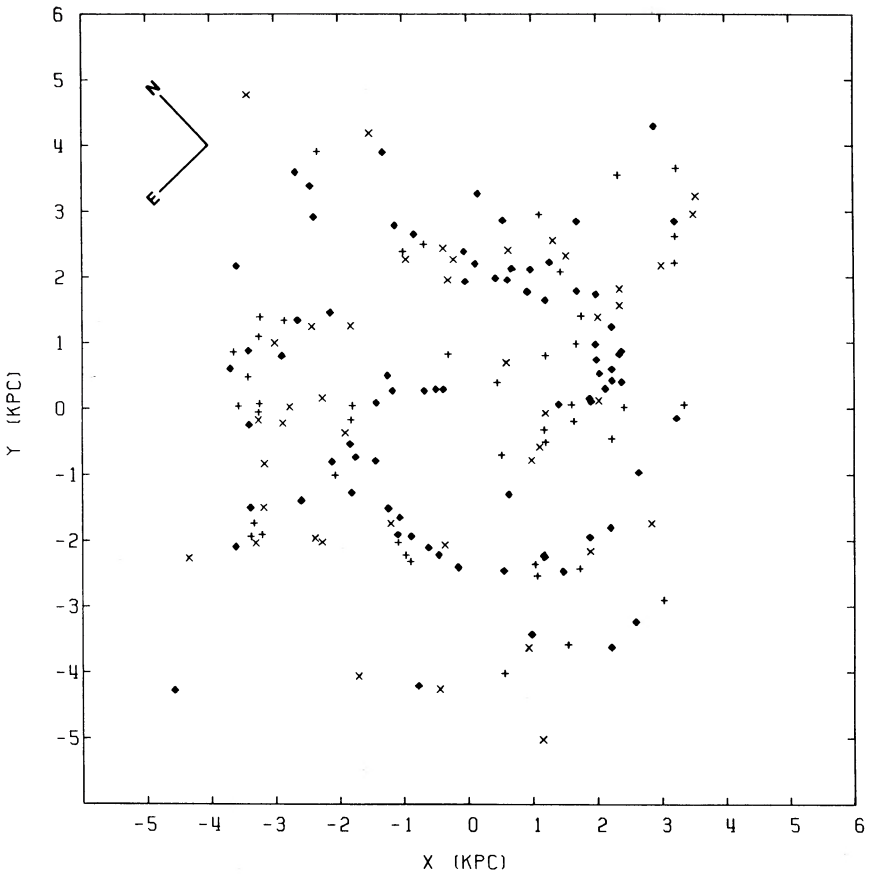

FIG. 6*b*

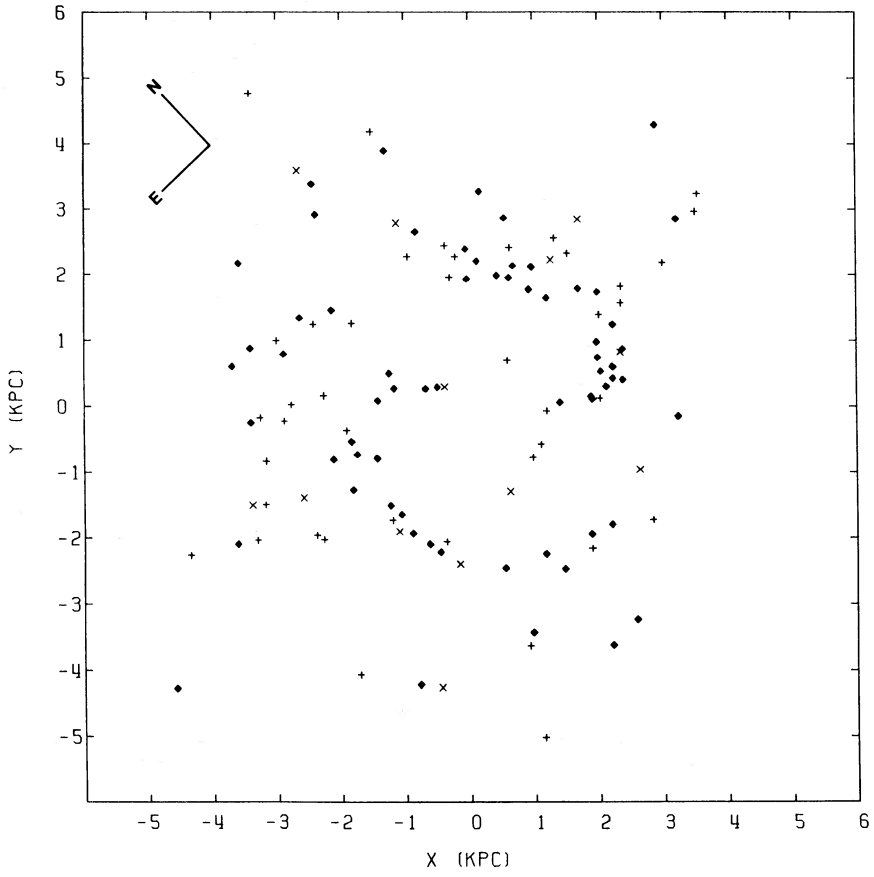

FIG. 6*c*

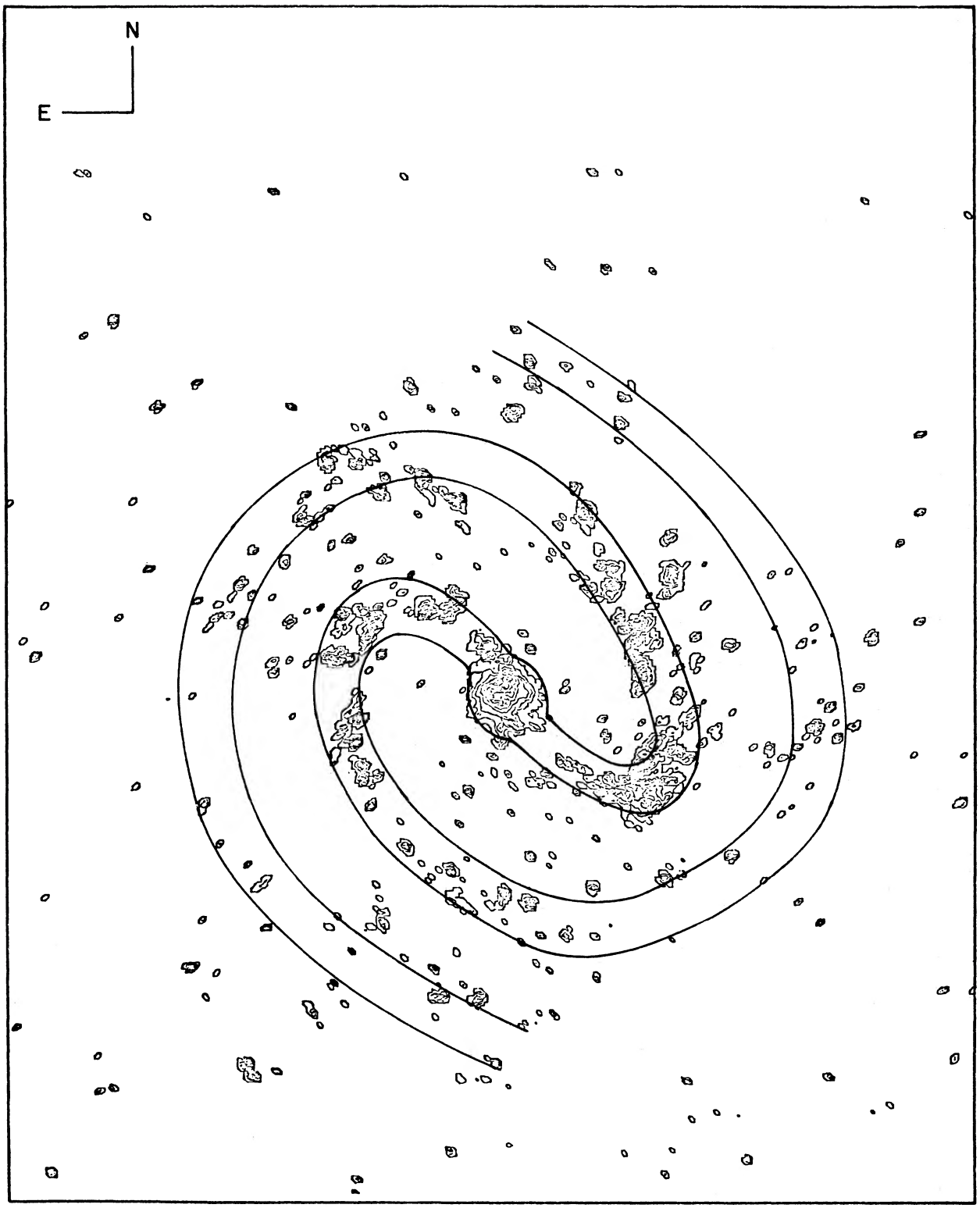

FIG. 7.—The asymmetric spiral arm system adopted for computing the contrast factor $\mathscr{R}$ listed in col. (4) of Table 3. This system is superimposed on a low resolution isophotal Hα map of M83 in the plane of the sky. The intensity scale is logarithmic, with contour interval equal to 0.5 mag. The average arm width is 650 pc.

TABLE 3

CONTRAST FACTOR $\mathscr{R}$ FOR M83

U (pc cm^{-2})	n	Asymmetric Arm System N_{in} (kpc^{-2})	Asymmetric Arm System $\mathscr{R}$	Symmetric Arm System N_{in} (kpc^{-2})	Symmetric Arm System $\mathscr{R}$
<115	112	2.34	2.92±0.36	2.21	2.76±0.38
> 70	268	5.78	3.12±0.38	5.67	3.07±0.41
>115	156	3.45	3.27±0.40	3.46	3.30±0.44
>150	113	2.52	3.30±0.37	2.60	3.64±0.53
> 200	74	1.93	5.08±0.54	1.96	5.51±0.78

H II regions suffering high extinction, and (*ii*) faulty assignment of H II regions to nongiant versus giant categories. The latter problem does not affect our distributions for M33 since here giant H II regions are defined by radio data. For M83 we have only optical data and use Talbot's statistical correction for extinction. It is therefore encouraging that both galaxies exhibit the same type of radial behavior, i.e., a narrower distribution of giant regions than of nongiant regions. On the other hand, problem (*i*) could influence the comparisons in both galaxies. For example, suppose that we have the true distribution of giant H II regions but that internal absorption in nongiant H II regions is larger than assumed at R_{peak}, the peak in the surface number density of giant H II regions, and falls off more steeply for $R > R_{peak}$. Then we would have systematically underestimated the number of nongiant H II regions near R_{peak} relative to those in the outer parts of the galaxy. We assume that this is not the case.

Assuming that the observed distributions represent the true distributions, we next use various statistical tests to compare the radial distribution of nongiant H II regions with that of giant H II regions in each galaxy. For each of the two galaxies, the χ^2 test applied to contingency tables gives the probability P_χ that the giant and nongiant H II regions represent samples from two different populations. For the range of galactocentric distance $R = 0.5$–7.0 kpc in M83, we obtain $P_\chi = 96\%$, and for $R = 0.0$–6.0 kpc in M33, $P_\chi = 90\%$, supporting our hypothesis. Roberts, Roberts, and Shu (1975) conclude that in M33 a classical spiral density wave would extend from $R = 0.0$ kpc to corotation at $R_c = 2.8$ kpc. This is the region where the bright optical arms IS and IN (defined by Sandage and Humphreys 1980) are located. If for M33 we consider only the range $R =$ 0.0–3.0 kpc (which includes R_{peak}), then we find that the distribution of nongiant regions is rather similar to the distribution of giant regions; in fact, P_χ is then less than 10%. In this respect M33 is unlike M83, where the sharp peak in the distribution of giant regions has no counterpart in the distribution of nongiant regions.

For each galaxy we next compute the centroid $\langle R \rangle$ and the rms scale S_R of each radial distribution, where

$$\langle R \rangle = \frac{1}{n} \sum_{i=1}^{n} R_i, \tag{2}$$

$$S_R^2 = \frac{1}{n-1} \sum_{i=1}^{n} (R_i - \langle R \rangle)^2, \tag{3}$$

and n is the number of H II regions in the sample. Table 4 indicates that in both M83 and M33, the values for $\langle R \rangle$ and S_R are smaller for the distribution of giant H II regions than for the distribution of nongiant H II regions. For the giant H II region population, the values of $\langle R \rangle$ and S_R appear to be insensitive to whether we include all regions with $U > 115$ pc cm^{-2} or only those with $U > 150$ pc cm^{-2}. We apply two nonparametric tests to the hypothesis that the scale S_R is larger for nongiant than for giant H II regions. Let P_J equal the probability from the Miller-Jackknife test (see, for example, Hollander and Wolfe 1973) and P_M, the probability from the Moses Ranklike test that this hypothesis is true. For M83 we obtain values of $P_J = 91\%$ and $P_M = 89\%$, and for M33 $P_J = 97\%$ and $P_M = 96\%$. Thus we conclude that the rms scale is larger for the distribution of nongiant regions. In the next section we compute *e*-folding lengths for the observed radial distributions and compare with the predictions of various models.

V. COMPARISON WITH SPIRAL DENSITY WAVE AND STOCHASTIC MODELS

Do the observed radial distributions of H II regions agree with those predicted by either spiral density wave (SDW) theory or by stochastic models for star formation?

Kaufman (1981) finds that in M33 the radial gradient in the distribution of giant regions out to corotation is similar to that predicted by a SDW. In this model the predicted surface number density of H II regions is

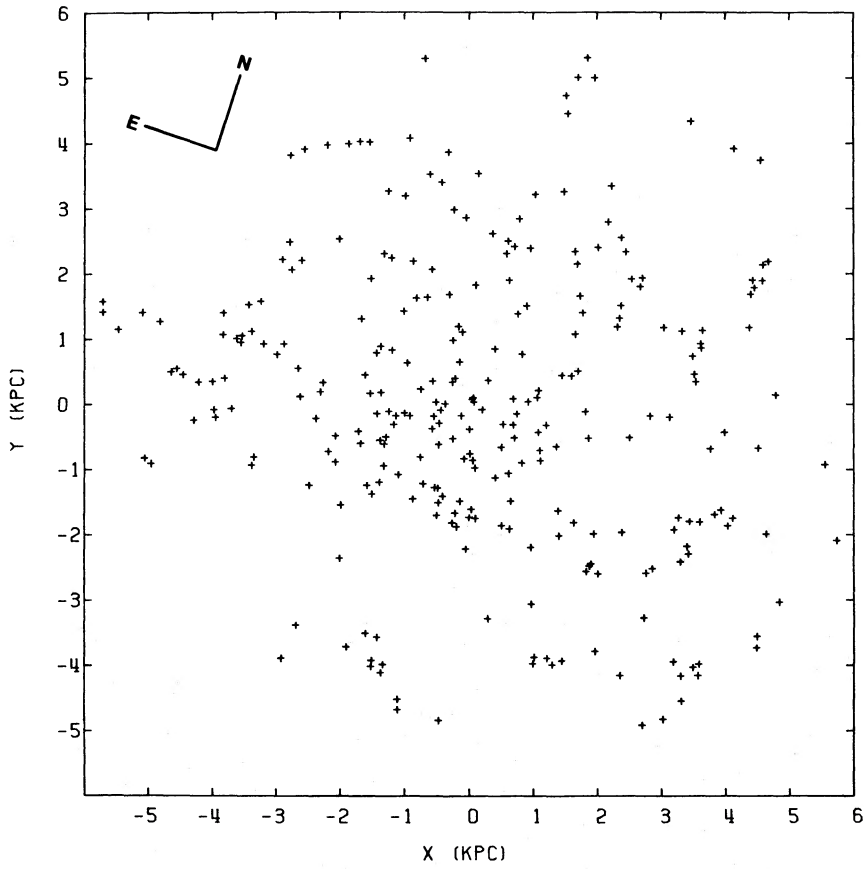

FIG. 8*a*

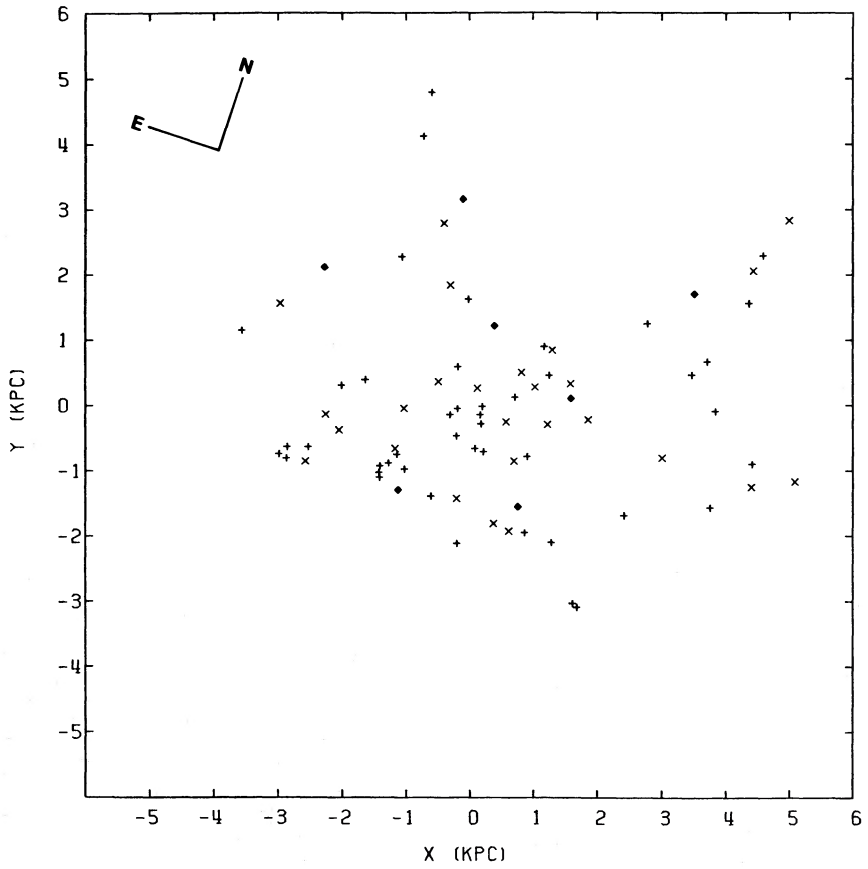

FIG. 8*b*

FIG. 8.—(*a*) The distribution of nongiant H II regions ($U < 115$ pc cm^{-2}) in the plane of M33. These are taken from the list of Boulesteix *et al.* (1974). (*b*) The distribution of giant H II regions ($U > 115$ pc cm^{-3}) in the plane of M33. These are taken from the radio observations of Israel and van der Kruit (1974). The symbols have the same meaning as in Fig. 6*b*.

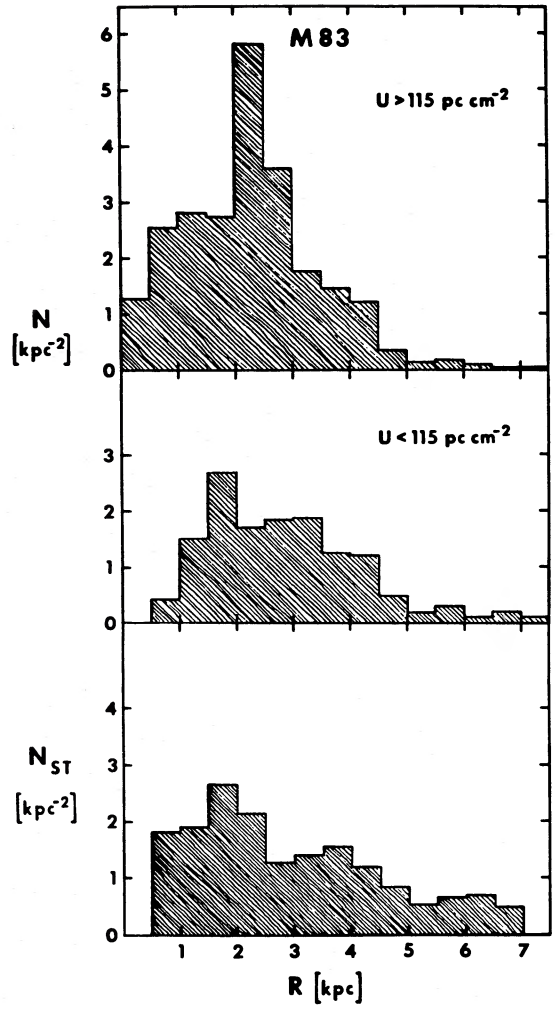

FIG. 9.—The two upper plots show the radial distributions in M83 of giant ($U > 115$ pc cm^{-2}) and nongiant ($U < 115$ pc cm^{-2}) H II regions, respectively. The bottom plot shows the radial variation of N_{st}, the stellar birth rate per kpc^2 predicted by a stochastic star formation model. N_{st} has been normalized to agree with the other two curves at $R = 4.0$–4.5 kpc.

taken as

$$N_{sp} \propto \sigma_g [\Omega(R) - \Omega_p], \quad (4)$$

where σ_g is the surface density of atomic plus molecular hydrogen, $\Omega(R)$ is the angular rotation speed, and Ω_p is the pattern speed. In equation (4) and in equation (5) below, the σ_g factor represents the amount of matter available for new star formation. For M33, we take σ_g equal to σ(H I), the surface density of atomic hydrogen, because only an upper limit on the amount of molecular hydrogen, i.e., $H_2/H\ I < 0.4$ (Young and Scoville 1982), is available. In making the following comparisons between M33 and a SDW model, we restrict consideration to the central region, $R = 0.2$–2.6 kpc, where a global spiral pattern appears. For the model we use the rotation curve and H I distribution from Rogstad, Wright, and Lockhart (1976) and Newton (1980) and take $\Omega_p = 32$ km s^{-1} kpc^{-1} (i.e., corotation $R_c = 2.8$ kpc) from Roberts, Roberts, and Shu (1975). We fit the observed and predicted distributions to exponentials $N \propto e^{-AR}$. For this central region, values of A, the inverse of the e-folding length, are listed in rows (1)–(3) of Table 5. The value of A for the SDW model agrees with the value obtained for the distribution of giant regions but is

TABLE 4

$\langle R \rangle$ AND S_R FOR H II REGION POPULATIONS IN M33 AND M83

Galaxy	U (pc cm^{-2})	n	$\langle R \rangle$ (kpc)	S_R (kpc)
M83	<115	126	3.56	1.60
	>115	170	2.94	1.34
	>150	124	2.94	1.36
M33	<115	290	2.99	1.62
	>115	78	2.24	1.39
	>150	33	2.24	1.38

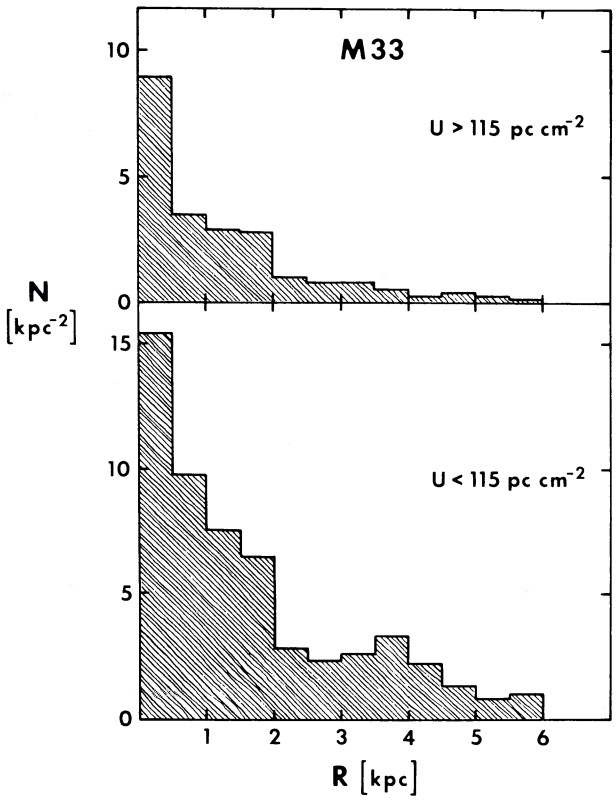

FIG. 10.—The radial distribution functions for giant ($U > 115$ pc cm^{-2}) and nongiant ($U < 115$ pc cm^{-2}) H II regions in M33.

TABLE 5

THE INVERSE OF THE *e*-FOLDING LENGTH OF PREDICTED AND OBSERVED RADIAL DISTRIBUTIONS

Row	Galaxy	Distribution	R (kpc)	A[a] (kpc^{-1})
(1)	M33	Giant regions	0.2–2.6	1.04 ± 0.23
(2)	M33	Nongiant regions	0.2–2.6	0.76 ± 0.08
(3)	M33	N_{sp} ($R_c = 2.8$ kpc)	0.2–2.6	1.10 ± 0.11
(4)	M33	Nongiant regions	3.5–6.0	0.67 ± 0.13
(5)	M33	N_{st}	3.5–6.0	0.54 ± 0.05
(6)	M33	Giant regions	0.0–5.5	0.74 ± 0.06
(7)	M33	Nongiant regions	0.0–5.5	0.50 ± 0.05
(8)	M33	σ_{tot}	0.5–5.5	0.51 ± 0.01
(9)	M83	Giant regions	2.0–4.0	1.01 ± 0.12
(10)	M83	Nongiant regions	1.5–4.0	0.29 ± 0.11
(11)	M83	N_{sp} ($R_c = 4.3$ kpc)	2.0–4.0	1.37–0.07
(12)	M83	N_{sp} ($R_c = 4.7$ kpc)	2.0–4.0	1.08 ± 0.01
(13)	M83	N_{sp} ($R_c = 5.0$ kpc)	2.0–4.0	0.94 ± 0.01
(14)	M83	N_{st}	1.5–4.0	0.30 ± 0.15
(15)	M83	Giant regions	2.0–6.0	1.11 ± 0.12
(16)	M83	Nongiant regions	1.5–6.0	0.63 ± 0.11
(17)	M83	N_{sp} ($R_c = 6.9$ kpc)	2.0–6.0	0.63 ± 0.04
(18)	M83	σ_{tot}	1.5–6.0	0.41 ± 0.02

[a] The uncertainties listed are statistical errors.

larger than the value for the distribution of nongiant regions in the same range of R. From a χ^2 test, we find a probability of at least 85% that the observed radial distribution of giant regions in this part of M33 is determined by the SDW model of equation (4).

The *e*-folding length for the distribution of giant regions in M83 (see rows [9] and [15] in Table 5) is approximately the same as the *e*-folding length for the distribution of giant H II regions in the central region of M33 discussed above. To calculate N_{sp} we combine Comte's (1981) velocity data and the rotation curve obtained by de Vaucouleurs, Pence, and Davoust (1983) for $R \leq 4.5$ kpc with the lower resolution 21 cm rotation curve of Rogstad, Lockhart, and Wright (1974) for larger R. We take $\sigma_g \propto e^{-0.14R}$ from Talbot (1980).

There is some disagreement in the literature about where to place corotation in M83: estimates range from 2.7 kpc (Jensen, Talbot, and Dufour 1981, plus the rotation curve of de Vaucouleurs *et al.*) to 4.3 kpc (Kormendy and Norman 1979) to 6.9 kpc (Talbot 1980). The value $R_c = 2.7$ kpc pertains to a model (e.g., see Schwarz 1981) in which the spiral shock goes from corotation to the outer Lindblad resonance. In this case, equation (4) does not apply. Kormendy and Norman chose $R_c = 4.3$ kpc as the maximum radius of the global pattern seen on large scale plates. Equation (4) then gives the value of A listed in row (11) of Table 5. The predicted distribution is steeper than the observed distribution of giant regions and much steeper than the distribution of nongiant regions (see rows [9] and [10]). However, if we take R_c as the peak of the rotation curve (that is, $R_c = 4.7$–5.0 kpc), then the predicted value of A would agree well with that for the distribution of giant regions (compare rows [9], [12], and [13]). At the other extreme, Talbot (1980) selected $R_c = 6.9$ kpc to represent the maximum extent of Hα emission from the disk. As one can see from rows (15)–(17), the predicted value of A would then agree well with the value obtained for the distribution of nongiant regions over the range $R =$ 2–6 kpc, but would be appreciably smaller than the value obtained for giant regions. Thus, if equation (4) applies, we appear to have two possible choices for R_c in M83, depending on whether we wish to fit the giant regions or nongiant regions. We shall return to this question after discussing stochastic models.

We next compare the observed radial distributions in both galaxies with those of stochastic models. In the purely stochastic models of Gerola and Seiden (1978), stars are produced by a combination of sporadic and sequential modes of star formation. The radial star formation gradient is then governed mainly by shear. Seiden and Gerola (1979) compute the radial variation of $B_{st}(R)$, the relative star formation rate per unit gas density, for a stochastic model with $d\Omega/dR \propto R^{-2}$. We shall compare the observed distributions with their curve for an appropriate range of R. Then, since the mass distribution in the galaxy determines its rotation curve, we shall compare the observed distributions with the surface mass distribution in the disk.

For the stochastic model, we take the predicted surface number density of H II regions to be

$$N_{st} \propto B_{st}\sigma_g. \quad (5)$$

We try to select a value for R_G, the galactic radius of the outermost ring in the stochastic model, so that (*i*) very few H II regions have $R > R_G$, and (*ii*) peaks in the predicted distribution lie close to peaks in the observed distribution. For each of the galaxies, we have chosen $R_G = 7.5$ kpc. We use $B_{st}(R)$ from Seiden and Gerola (1979) and σ_g from Talbot (1980) to obtain the binned version of N_{st} for M83 shown in Figure 9; a similar function is obtained for M33.

For both M83 and M33, the stochastic curve is more similar to the observed distribution of nongiant regions than to the observed distribution of giant H II regions. Quantitative comparisons should be made only for the range of R where $d\Omega/dR \propto R^{-2}$. From Comte's (1981) data on the velocity field of M83, Rumstay (1982) finds that $d\Omega/dR$ behaves approximately like R^{-2} (i.e., $v \approx a_0 + a_1 R$) for $R = 1.75$–4 kpc. For the appropriate range of R (adjusted slightly to start at the main peak of each distribution), rows (9), (10), and (14) of Table 5 list values of the inverse *e*-folding length A for the various distributions. The values of A obtained for the nongiant regions and for the stochastic model are consistent. The distribution of giant regions drops off much more steeply than either of these.

The radial distributions of nongiant regions in M83 and the stochastic model both show some indication of a secondary peak beyond the main peak. This is also true for the distribution of nongiant regions in M33. In the multi-armed outer region ($R > 3.5$ kpc), the rotation curve of M33 is nearly flat. From the values of A given in rows (4) and (5) of Table 5, we see that the *e*-folding lengths of the stochastic model and the distribution of nongiant regions are similar for $R = 3.5$–6 kpc in M33.

We next compare the radial distributions of H II regions, from the main peak of each curve outward, with the radial variation of σ_{tot}, the total surface mass density. From Comte's (1981) data, Rumstay (1982) finds that σ_{tot} in M83 has an *e*-folding length of 2.45 ± 0.11 kpc. For M33 we use σ_{tot} from the mass model of Warner, Wright, and Baldwin (1973). For M33 we note that (*i*) there is good agreement between the *e*-folding lengths of σ_{tot} and the distribution of nongiant regions (see rows [6]–[8] of Table 5), and (*ii*) σ_g shows no systematic trend with R for the range of R considered here. In M83, σ_g is proportional to $e^{-0.14R}$, and the distribution of nongiant regions is slightly steeper than σ_{tot} (see rows [15], [16], and [18]). If this difference is real, it suggests that the surface number density of nongiant H II regions may behave like $\sigma_{tot}\sigma_g$: in both galaxies the distribution of nongiant regions has, on the average, about the same *e*-folding length as $\sigma_{tot}\sigma_g$ has. This is clearly not the case for the overall distribution of giant regions. Within the context of the stochastic model, the σ_{tot} factor can be viewed as representing the effect of the rotation curve on sequential star formation, while σ_g is the gas available for forming new stars.

We conclude that the radial distribution of nongiant H II regions is consistent with the predictions of the stochastic model. In addition, the multiple spiral features in the plots of nongiant regions in M33 and M83 resemble what might be expected for a stochastic process. On the other hand, the *e*-folding lengths for the distributions of giant regions in both galaxies are significantly smaller than for the stochastic model of equation (5). In M33 the radial distribution of giant regions is consistent with a SDW for the annulus where the global pattern appears. Since a SDW model is not necessary to explain the distribution of nongiant regions in M83, we choose to place corotation for M83 near the peak of the rotation curve, and thus fit the radial distribution of giant regions in this galaxy, also, with a SDW model.

VI. INTERPRETATION

We consider the following results of §§ IV and V for M83 and M33.

A. Compared to giant H II regions, nongiant regions are less concentrated in a two-armed pattern and have a broader radial distribution in the galaxy.

B. The radial distribution of nongiant regions in the galaxy is consistent with stochastic star formation while the steeper radial distribution of giant regions appears consistent with a spiral density wave.

There is some indication (Fich and Blitz 1983) that in our Galaxy, nongiant and giant regions may differ in radial distribution in the same sense as in M83 and M33.

In our Galaxy, H II regions are closely associated with molecular clouds (see Israel 1978 and Blitz 1980). Emphasis has been put on the proximity of OB associations to giant molecular clouds (GMCs). The question of whether OB stars form in molecular clouds of mass intermediate between GMCs and dark clouds is still an open one. Blair (1976) finds that many Sharpless H II regions are associated with intermediate-mass molecular clouds, but L. Blitz (1982, private communication) feels that because of incomplete mapping, Blair's mass estimates should be regarded as lower limits. We shall assume that H II regions in M33 and M83 are also related to molecular clouds. Giant molecular clouds in our Galaxy and M31 are observed to occur preferentially in the spiral arms (Stark 1979; Boulanger, Stark, and Combes 1981; Linke 1982), while molecular clouds of intermediate mass in our Galaxy are not significantly concentrated in the spiral arms (Stark 1979). Qualitatively, the difference in azimuthal distribution between giant and intermediate-mass molecular clouds in our Galaxy is somewhat similar to the difference in azimuthal distribution between giant and nongiant H II regions in M83 and M33. However, as noted in § IV, even nongiant H II regions show some concentration to the spiral arms. This comparison suggests that in these galaxies

giant H II regions occur in GMCs, while nongiant H II regions occur in both GMCs and in molecular clouds of lower mass. The latter may be fragments of disrupted GMCs. In both the dust-lane collapse model of Elmegreen (1979) and the cloud-coalescence model of Casoli and Combes (1982), GMCs form primarily in the main spiral arms because of the compression by a spiral density wave.

Our results A and B above are consistent with the following speculations about star formation.

The spiral density wave is responsible for producing most of the GMCs in which giant H II regions may eventually occur. Once star formation has been initiated in a GMC, subsequent generations can form by sequential star formation mechanisms. But, as discussed in Kaufman (1979, 1981), the efficiency for producing large OB associations by sequential star formation is less than 1. This results, in part, because the energy input from stars (see Blitz and Shu 1980) or from collisions with small clouds (Leisawitz and Bash 1982) tends to disperse the GMC. The next passage through the SDW produces a new generation of GMCs and revives the formation of large OB associations.

Thus, stars in giant H II regions are likely to owe their existence to a spiral density wave plus sequential star formation. Nevertheless, in the outer parts of galaxies such as M33, there are giant H II regions that are not connected with a classical density wave.

Some nongiant H II regions are found in clouds where star formation has been triggered directly by a density wave. However, in most nongiant H II regions, star formation has resulted from the combination of sporadic and sequential mechanisms described in stochastic models. Since nongiant H II regions are more numerous than giant regions, result B implies that stochastic star-forming processes are much more effective in producing OB stars in small groups than in the larger groups that form giant H II regions. This can be understood, if, for example, (*i*) stochastic star formation is more relevant to star formation in molecular clouds of intermediate mass (e.g., in fragments of GMCs), and (*ii*) molecular clouds of intermediate mass are more common and have a more extensive distribution than GMCs in the galaxy. In particular, random galactic supernovae and sporadic star-forming mechanisms, such as cloud-cloud collisions, may be more successful in triggering star formation in molecular clouds of intermediate mass than in GMCs.

VII. CONCLUSIONS

The observed spatial distribution of H II regions in M83 and M33 indicates that massive stars in most of the high luminosity H II regions are formed by different mechanisms than in most of the low luminosity H II regions. Specifically, we have found the following results.

1. The global distribution of nongiant H II regions in the plane of the galaxy is less concentrated both in azimuth and as a function of galactocentric radius than the distribution of giant H II regions.

2. The radial gradient in the global distribution of nongiant H II regions agrees with the predictions of a stochastic model for star formation.

3. The steeper radial distribution of giant H II regions appears consistent with a spiral density wave.

We conclude that stochastic processes are more important for producing stars in nongiant H II regions, whereas a spiral density wave is more relevant for star formation in giant H II regions.

For H II regions in M83, the observed luminosity and diameter distribution functions may provide additional evidence for two subpopulations of H II regions. For highly luminous H II regions in M83 (that is, regions with values of the excitation parameter U in excess of 150–200 pc cm^{-2}), the luminosity and diameter distribution functions are each well represented by power laws with power law indices close to the values that Kennicutt and Hodge (1980) obtained for highly luminous H II regions in NGC 628. Less luminous H II regions in M83 have a flatter luminosity function and a flatter diameter distribution function.

We thank R. J. Talbot for providing us with a copy of the computer tape containing the *UBVR* Hα maps of Talbot, Jensen, and Dufour. We thank R. J. Talbot, E. B. Jensen, R. Pennington, L. Blitz, and R. C. Kennicutt for their useful advice, and we thank C. J. Peterson for calling our attention to the paper by Comte.

REFERENCES

Baade, W. 1963, in *Evolution of Stars and Galaxies* (Cambridge: Harvard University Press), p. 63.
Blair, C. N. 1976, Ph.D. thesis, The University of Texas at Austin.
Blitz, L. 1980, in *Giant Molecular Clouds in the Galaxy*, ed. P. M. Solomon and M. G. Edmunds (Oxford: Pergamon Press), p. 1.
Blitz, L., and Shu, F. H. 1980, *Ap. J.*, **238**, 148.
Block, D. L. 1982, *Astr. Ap.*, **109**, 336.
Boulanger, F., Stark, A. A., and Combes, F. 1981. *Astr. Ap.*, **93**, L1.
Boulesteix, J., Courtès, G., Laval, A., Monnet, G., and Petit, H. 1974, *Astr. Ap.*, **37**, 33.
Carranza, G. J. 1968, *Bol. Asoc. Astr. Argentina*, No. 14, 38.
Casoli, F., and Combes, F. 1982, *Astr. Ap.*, **110**, 287.
Comte, G. 1981, *Astr. Ap. Suppl.*, **44**, 441.
Comte, G., and Monnet, G. 1974, *Astr. Ap.*, **33**, 161.
Condon, J. J., Condon, M. A., Gisler, G., and Puschell, J. J. 1982, *Ap. J.*, **252**, 102.
de Vaucouleurs, G. 1959, *Ap. J.*, **130**, 728.
_____. 1978, *Ap. J.*, **223**, 770.
_____. 1979, *A.J.*, **84**, 1270.
de Vaucouleurs, G., de Vaucouleurs, A., and Corwin, H. S., Jr., 1976, *Second Reference Catalogue of Bright Galaxies* (Austin: University of Texas Press).

de Vaucouleurs, G., Pence, W. D., and Davoust, E. 1983, *Ap. J. Suppl.*, **53**, 17.
Dufour, R. J., Talbot, R. J., Jensen, E. B., and Shields, G. A. 1980, *Ap. J.*, **236**, 119.
Elmegreen, B. G. 1979, *Ap. J.*, **231**, 372.
Fich, M. J., and Blitz, L. 1983, in *The Structure, Dynamics, and Kinematics of the Milky Way*, ed. W. H. Shuter (Dordrecht: Reidel), in press.
Georgelin, Y. M., and Georgelin, Y. P. 1976, *Astr. Ap.*, **49**, 57.
Gerola, H., and Seiden, P. E. 1978, *Ap. J.*, **223**, 129.
Habing, H. J., and Israel, F. P. 1979, *Ann. Rev. Astr. Ap.*, **17**, 345.
Hodge, P. W. 1974, *Pub. A.S.P.*, **86**, 845.
Hollander, M., and Wolfe, D. A. 1973, *Nonparametric Statistical Methods* (New York: John Wiley and Sons).
Israel, F. P. 1978, *Astr. Ap.*, **70**, 769.
_____. 1980, *Astr. Ap.*, **90**, 246.
Israel, F. P., and van der Kruit, P. C. 1974, *Astr. Ap.*, **32**, 363.
Jensen, E. B., Talbot, R. J., and Dufour, R. J. 1981, *Ap. J.*, **243**, 716.
Kaufman, M. 1979, *Ap. J.*, **232**, 717.
_____. 1981, *Ap. J.*, **250**, 534.
Kennicutt, R. C. 1979, *Ap. J.*, **228**, 394.
_____. 1981, *A.J.*, **86**, 1847.
_____. 1982, *A.J.*, **87**, 255.
Kennicutt, R. C., and Hodge, P. W. 1980, *Ap. J.*, **241**, 573.
Kormendy, J., and Norman, C. A. 1979, *Ap. J.*, **233**, 539.
Lada, C. S., Blitz, L., and Elmegreen, B. G. 1978, in *Protostars and Planets*, ed. T. Gehrels (Tucson: University of Arizona Press), p. 341.
Leisawitz, D., and Bash, F. 1982, *Ap. J.*, **259**, 133.
Lin, C. C., and Shu, F. H. 1964, *Ap. J.*, **140**, 646.
Linke, R. A. 1982, in *Extragalactic Molecules*, ed. L. Blitz and M. Kutner, (Green Bank, W.V.: Publications Division, NRAO), p. 87.
Mezger, P. G. 1970, in *IAU Symposium 38, The Spiral Structure of our Galaxy*, ed. W. Becker and G. Contopoulos (Dordrecht: Reidel), p. 107.
Mezger, P. G., and Henderson, A. P. 1967, *Ap. J.*, **147**, 471.
Newton, K. 1980, *M.N.R.A.S.*, **190**, 680.
Peimbert, M., Rayo, J. F., and Torres-Peimbert, S. 1975, *Rev. Mexicana Astr. Ap.*, **1**, 289.
Pennington, R., Talbot, R. J., and Dufour, R. J. 1982, *A.J.*, **87**, 1538.
Roberts, W. W., Roberts, M. S., and Shu, F. H. 1975, *Ap. J.*, **196**, 381.
Rogstad, D. H., Lockhart, J. A., and Wright, M. C. H. 1974, *Ap. J.*, **193**, 309.
Rogstad, D. H., Wright, M. C. H., and Lockhart, J. A., 1976, *Ap. J.*, **204**, 703.
Rumstay, K. S. 1982, *Bull. AAS*, **14**, 660.
Sandage, A., and Humphreys, R. M. 1980, *Ap. J.* (*Letters*), **236**, L1.
Sandage, A., and Tammann, G. A. 1974, *Ap. J.*, **190**, 525.
Schwarz, M. 1981, *Ap. J.*, **247**, 77.
Seiden, P. E., and Gerola, H. 1979, *Ap. J.*, **233**, 56.
Stark, A. A. 1979, Ph.D. thesis, Princeton University.
Talbot, R. J., Jensen, E. B., and Dufour, R. J. 1979, *Ap. J.*, **229**, 91.
Talbot, R. J., Jr. 1980, *Ap. J.*, **235**, 821.
Warner, P. J., Wright, M. C. H. and Baldwin, J. E. 1973, *M.N.R.A.S.*, **163**, 163.
Young, J. S. and Scoville, N. Z. 1982, *Bull. AAS*, **14**, 617.

MICHELE KAUFMAN: The Ohio State University, Department of Physics, 174 West 18th Avenue, Columbus, OH 43210

K. S. RUMSTAY: The Ohio State University, Department of Astronomy, 174 West 18th Avenue, Columbus, OH 43210